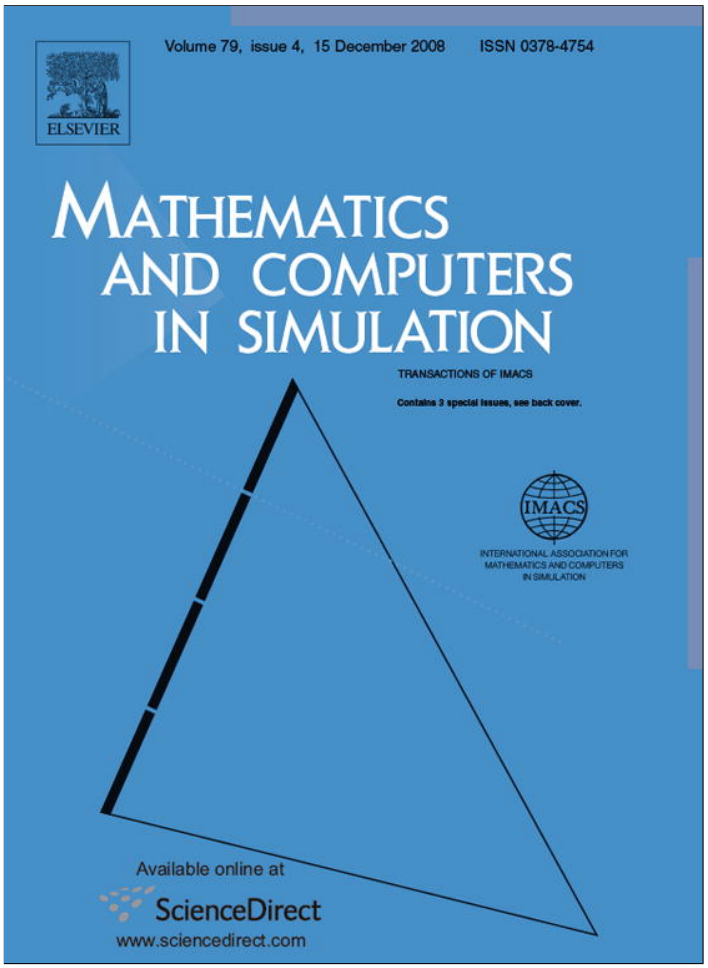

Available online at www.sciencedirect.com
ScienceDirect
Mathematics and Computers in Simulation 79 (2008) 972–979
MATHEMATICS AND COMPUTERS IN SIMULATION
www.elsevier.com/locate/matcom

Effect of band structure discretization on the performance of full-band Monte Carlo simulation

G. Karlowatz *, W. Wessner, H. Kosina

Institute for Microelectronics, TU Wien, Gußhausstraße 27-29/E360, 1040 Wien, Austria

Available online 17 February 2008

Abstract

Full-band Monte Carlo simulation offers a very accurate simulation technique, but is often limited by its high demand on computation time. The advantage of a numerical representation of the band structure over an analytical approximation is the accurate representation of the energy bands in the high energy regime. This allows accurate treatment of hot carrier effects in semiconductors. In this work we outline an efficient full-band Monte Carlo (FBMC) simulator and investigate the accuracy of simulation results for different meshing approaches for the Brillouin zone.

Keywords: Strained silicon; Electron transport; Electronic band structure; Full-band Monte Carlo; k-Space discretization

1. Introduction

The VIENNA MONTE CARLO SIMULATOR(VMC) [4] offers simulation algorithms for both bulk semiconductors and one-dimensional devices based on analytical and full-band models. Additionally, a fast zero-field algorithm is included [11]. VMC provides a comprehensive set of scattering models including phonon scattering, ionized impurity scattering, alloy scattering and impact ionization.

For FBMC simulations a numerical representation of the band structure in the unit cell of the reciprocal lattice, the so-called *Brillouin zone*, is used to capture the dependence of the carrier energy on the wave vector. Taking advantage of the periodicity and the symmetry properties of a crystal only a part of the band structure in the first Brillouin zone, the so-called *irreducible wedge* has to be considered [9]. For unstrained silicon with its diamond crystal structure this irreducible wedge is only 1/48 of the Brillouin Zone. Fig. 1 shows the first Brillouin zone and the irreducible wedge for unstrained silicon.

In this work, we describe the basic layout of a rejection algorithm used by VMC to select the final tetrahedron for a carrier after a scattering event occurred. It is shown why the use of tetrahedral meshes is convenient for this selection algorithm. Results of bulk simulations of unstrained silicon are shown, demonstrating the impact of different meshing strategies on simulation accuracy and computation time.

* Corresponding author.
E-mail addresses: karlowatz@iue.tuwien.ac.at (G. Karlowatz), wessner@iue.tuwien.ac.at (W. Wessner), kosina@iue.tuwien.ac.at (H. Kosina).

0378-4754/$32.00 © 2008 IMACS. Published by Elsevier B.V. All rights reserved.
doi:10.1016/j.matcom.2008.02.021

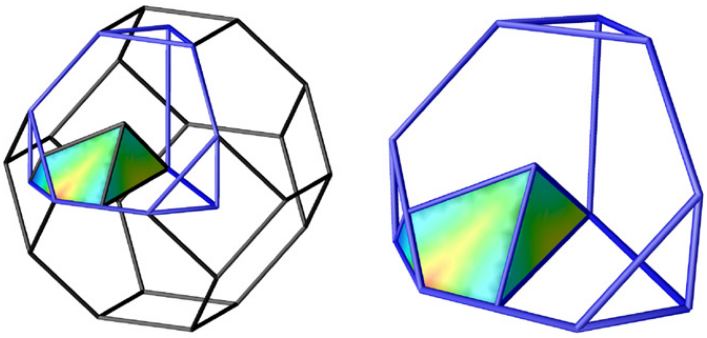

(a) Brillouin zone (b) First octant of the Brillouin zone

Fig. 1. Brillouin zone of silicon highlighting the first octant and the first irreducible wedge.

2. Efficient scattering algorithms

Special attention has been paid to keep the code efficient because the CPU time consumption of FBMC is often a drawback for practical use. One crucial point is to incorporate efficient scattering algorithms. In VMC scattering models with constant matrix elements are used [5], so that the scattering rates are proportional to the *density of states* (DOS) at the particle's final energy after scattering ϵ_f. Selection of a carrier state after scattering then relies mainly on fast calculation of the contribution to the DOS of the mesh elements including the particle's final energy. This is achieved by using tetrahedral mesh elements and linear interpolation of the energy within the mesh elements. The contribution to the DOS g_i of the i-th tetrahedron is proportional to the intersection of the energy iso-surface $A_i(\epsilon_f)$ [8,6].

$$g_i = \frac{1}{(2\pi)^3\hbar}\frac{A_i(\epsilon)}{|\mathbf{v}(\mathbf{k})|} \tag{1}$$

Here $\mathbf{v}(\mathbf{k})$ is the group velocity

$$\mathbf{v}(\mathbf{k}) = \frac{1}{\hbar}\nabla_{\mathbf{k}}\epsilon(\mathbf{k}) \tag{2}$$

which is constant within a tetrahedron. It can be precalculated and stored in a table. The whole DOS is given by

$$g(\epsilon_f) = \frac{1}{(2\pi)^3}\int_{BZ}\delta(\epsilon-\epsilon_f(\mathbf{k}))\,d^3k = \frac{1}{(2\pi)^3\hbar}\int_{A(\epsilon_f)}\frac{1}{|\mathbf{v}(\mathbf{k})|}\,d^2k = \sum_i g_i \tag{3}$$

One superior feature of tetrahedral meshes over cubical-meshes is that an energy iso-surface within the Brillouin zone is continuous.

The most time consuming task while performing a scattering event is the selection of a final tetrahedron containing the final energy ϵ_f. Several tables are calculated once at start time of the simulation to speed up this selection process.

- *Table of sorted tetrahedrons:* the tetrahedral mesh elements representing the considered part of the first Brillouin zone are sorted with respect to their lowest energy values. Additionally, the numbering of the vertices of each tetrahedron is sorted with respect to increasing energy levels.
- *Table of upper bounds for DOS:* the maximum DOS within all tetrahedrons within subsequent energy intervals is stored to build a table of upper bounds $\overline{\mathrm{DOS}}(\epsilon)$.
- *Upper bound for energy differences:* the largest energy difference within tetrahedrons in a specific energy interval is stored for subsequent energy intervals to build a list of upper bounds $\Delta\epsilon_{\max}(\epsilon)$.

After a scattering event is evaluated the final energy ϵ_f of the scattered particle is known and so the search for a final tetrahedron after scattering can be constricted to the tetrahedrons containing ϵ_f. Actually only tetrahedrons with a

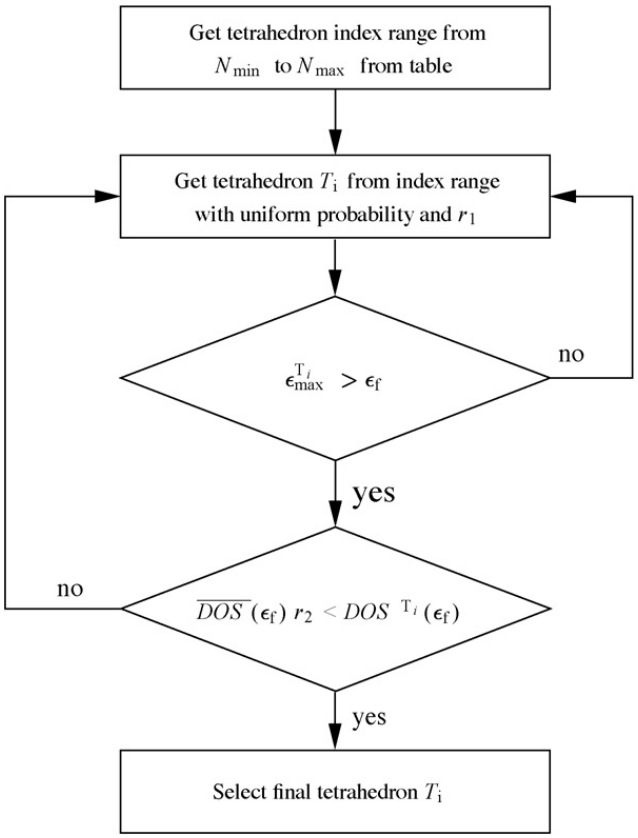

Fig. 2. Rejection technique for the selection of the final state in k-space. r_1 and r_2 are uniformly distributed random numbers between zero and one.

minimum energy in the range between ϵ_{min} and ϵ_{max} from the table of sorted tetrahedrons are considered in this search.

$$\begin{aligned} \epsilon_{min} &= (\epsilon_f - \Delta\epsilon_{max}(\epsilon_f)) \\ \epsilon_{max} &= \epsilon_f \end{aligned} \tag{4}$$

The corresponding table indices N_{min} and N_{max} are calculated by a binary search. Then a tetrahedron T_i is chosen randomly from this interval. There is a small number of tetrahedrons in the considered interval which do not contain ϵ_f. These are sorted out within a first rejection step. During a second rejection step the DOS within the tetrahedron has to be evaluated. Fig. 2 shows a flow-chart of the selection procedure with its two step rejection technique. Since the whole procedure is repeated until the second rejection step is passed, $g_i(\epsilon_f)$ has to be evaluated frequently during the simulation. In this task tetrahedron meshes perform very efficient because of the efficient way to calculate a tetrahedron's contribution to the DOS.

3. Representation of the band structure in momentum-space

In VMC the first octant of the first Brillouin Zone is meshed to represent the band structure of relaxed and biaxially strained silicon. Because an octant is a larger volume than the irreducible wedge, this approach obviously increases memory consumption. However, it simplifies the manipulations needed when particles reach a boundary. The energy bands are calculated for the irreducible wedge using the empirical pseudopotential method [10] and then transformed by coordinate permutation to completely fill the first octant. Two approaches of mesh generation are used in the VMC, one providing structured and another providing unstructured tetrahedral meshes.

3.1. Structured tetrahedral mesh

This mesh is based on an octree-based approach. The basic idea behind this method is to divide the whole domain to be meshed into cubes and afterwards this cubes are divided into six tetrahedrons. To mesh the {1 1 1} surface of the

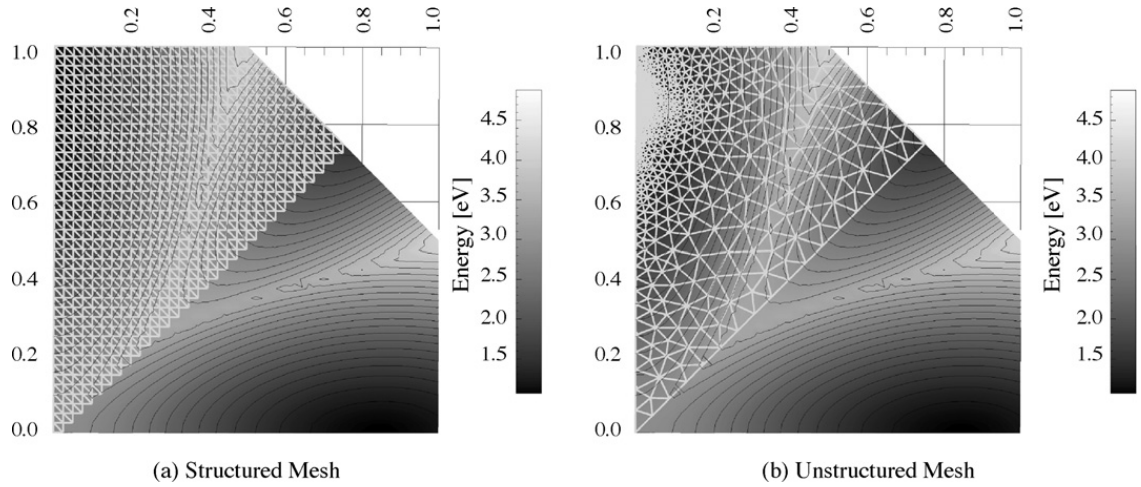

Fig. 3. $k_x - k_y$ plane of the first conduction band in the first Brillouin Zone with (a) structured and (b) unstructured meshes, shown is only one octant.

Brillouin zone either one or five tetrahedrons have to be cut away from the six tetrahedrons forming one cube. The result is a structured tetrahedral mesh, whose surface is conform with the Brillouin zone boundary.

Fig. 3 (a) shows the $k_x - k_y$ plane of the first octant of the Brillouin zone with the contour plot of the energy of the first conduction band. The main drawback of the octree approach is, that it is very challenging to implement a sufficient and flexible refinement strategy to adjust different mesh densities. In [2], an octree algorithm is proposed which can deal with different mesh densities, but the refinement zone is limited to a cubical region and therefore not very flexible.

3.2. Unstructured tetrahedral mesh

A very flexible way of generating unstructured meshes is to use a mesh generator which can handle arbitrary point clouds with different point densities. In this particular work DELINK[3] was used to generate an initial, very coarse, unstructured mesh. For different energy bands this initial mesh was refined by the so-called *tetrahedral bisection* method. The basic idea of this method is to insert a new vertex on a particular edge, the *refinement edge*, of a tetrahedron, and to cut the tetrahedron into two pieces.

In literature, one can find different improvements and specifications for this algorithm (see, for example [1]). One common problem is the detection of the refinement edge, as supporter for the new vertex. In a mesh, tetrahedrons are not isolated and inserting a new vertex influences the whole refinement edge batch of the tetrahedron if the conformity of the mesh after the refinement step should be kept, which is normally the case. To guarantee good shaped elements, a recursive refinement mechanism was chosen. This approach produces very regular, almost isotropic elements. Regimes of high point densities are pre-defined by the known positions of the band-minima in the Brillouin zone.

3.3. Recursive refinement algorithm

To guarantee a conforming mesh during the refinement procedure, all tetrahedrons sharing a common refinement edge have to be divided. A tetrahedron is said to be *compatibly divisible* if its refinement edge is either the refinement edge of all other tetrahedrons sharing that edge or the edge is part of the boundary of the domain. If a tetrahedron is compatibly divisible, we divide the tetrahedron and all other refinement edge sharing tetrahedrons simultaneously. If a tetrahedron is not compatibly divisible, we ignore it temporarily and divide a neighbor tetrahedron by the same process first. This leads to the atomic algorithm [7]. Fig. 4 illustrates the recursive refinement process, where one new vertex is inserted.

As an input to the mesher, regimes of high point densities are pre-defined by the known positions of the band-minima in the Brillouin zone of silicon. The dimension of this regime is chosen such that the shifted band-minima of strained silicon are considered and so the same mesh structure is usable with recalculated energy values for different amounts of strain.

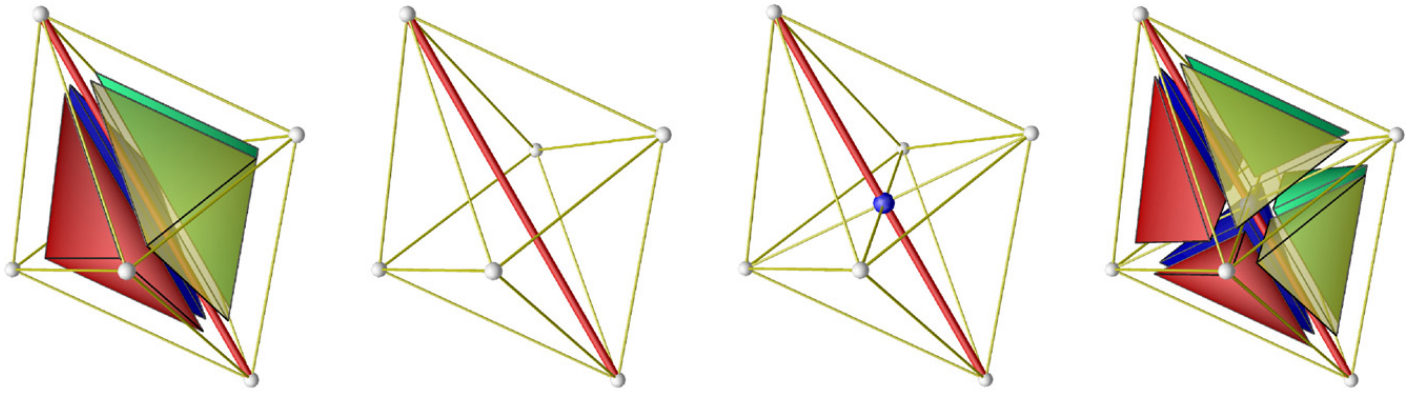

(a) Four tetrahedrons. (b) The refinement edge. (c) New vertex. (d) Eight tetrahedrons.

Fig. 4. The recursive refinement procedure involving four tetrahedrons with one common refinement edge.

Table 1
Parameter values of the meshes used for the first conduction band and CPU time consumption for electron velocity simulations

Group	Granularity	Data structure points	Tetrahedrons	Build-up time	200 kV/cm	0.1 kV/cm
Structured	Fine	278 166	1 536 134	12′19″	18′55″	14′49″
	Coarse	37 286	192 618	2′26″	4′51″	3′12″
Unstructured	Fine	39 330	180 294	1′45″	4′57″	3′54″
	Coarse	20 346	88 938	1′26″	4′11″	3′01″

4. Results

Two meshes, a fine one and a coarse one were generated for each the structured and the unstructured mesh type. The number of points and tetrahedrons in the first conduction band of these meshes are shown in Table 1.

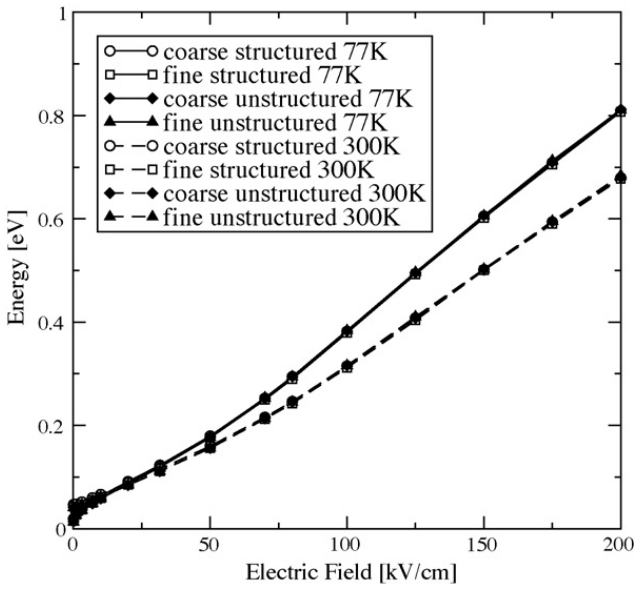

Fig. 5. Electron mean energy versus field along [1 0 0] direction at 77 K and 300 K.

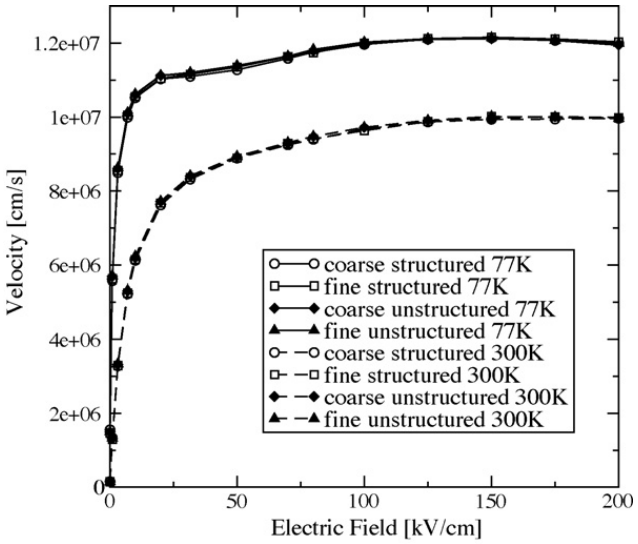

Fig. 6. Electron velocity versus field along [1 0 0] direction at 77 K and 300 K.

4.1. High field behavior

Fig. 5 shows the mean electron energy as a function of the electric field for bulk silicon for both structured and unstructured tetrahedral meshes. As the curves for 300 K and also for 77 K are grouped very close together above 10 kV/cm, it can be concluded that for practical purposes the accuracy of the results in the high field regime is about the same for all meshes. Fig. 6 shows a similar result for the velocity as a function of the electric field. These results demonstrate that the unstructured meshes perform very well in the high energy regimes, despite they contain less mesh elements than the structured meshes in that areas.

4.2. Low field behavior

Fig. 7 shows the normalized mean energy of electrons obtained from FBMC simulation at thermal equilibrium. The result for the unstructured meshes are in good agreement and converge for low temperatures to the theoretical equilibrium value of $3k_B T/2$. While the fine structured mesh is sufficiently accurate at high temperatures, both structured

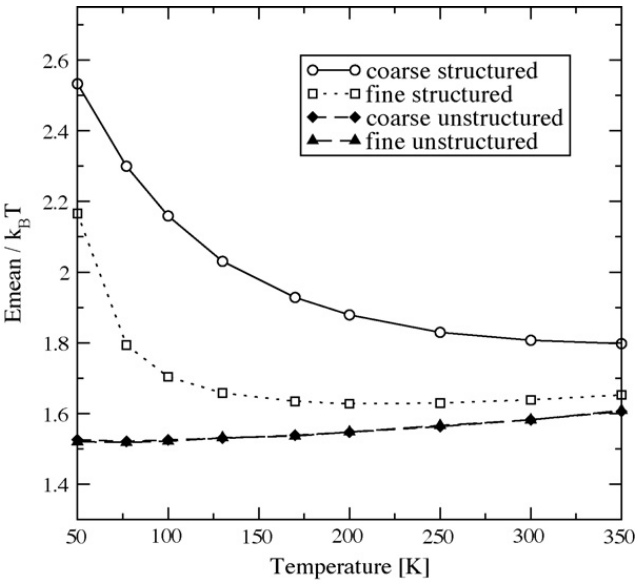

Fig. 7. Normalized mean energy of electrons at thermal equilibrium versus temperature.

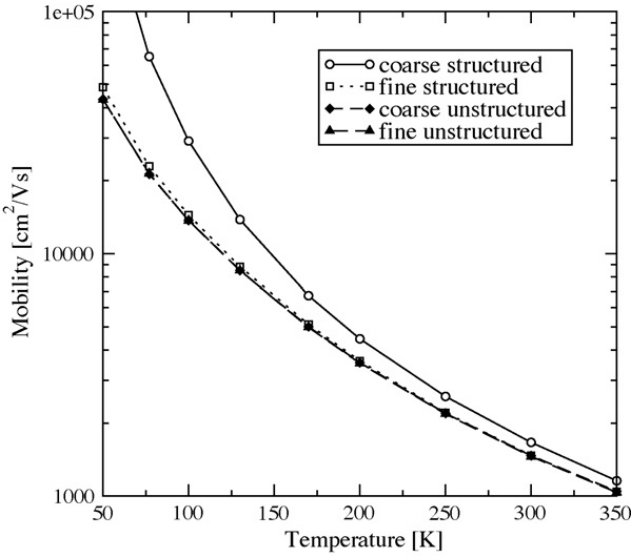

Fig. 8. Low field mobility of electrons versus temperature.

meshes fail completely at low temperatures. Fig. 8 shows the low field mobility of electrons. Again the coarse structured mesh fails, while fine structured mesh is in fair agreement with the unstructured meshes.

4.3. Computional costs

Table 1 gives an overview about computation times for different meshes. The computation times are separated into the mesh data structure build-up times, which is required once at the beginning of the simulation, and two typical field point calculations, one in the low field regime at 0.1 kV/cm and a second one at 200 kV/cm. For every field point calculated the total amount of scattering events was set to 5×10^6. For the calculations a commercially obtainable Intel® Pentium® 4 CPU with 2.4 GHz was used and the user process CPU time was measured.

One can clearly observe that the CPU time consumption is high for the structured meshes. This is mainly due the higher build-up times. With its much higher amount of mesh elements in the fine structured mesh, it takes a long time to compute the precalculated tables shown in the last section. The unstructured fine mesh is approximately in the same range as the coarse structured mesh, but one has to keep in mind, that the structured mesh fails completely for average kinetic energy at temperatures less than room temperature, where the coarse unstructured mesh still gives reasonable results.

5. Conclusion

It has been shown that tetrahedral meshes are a convenient choice for meshing the Brillouin Zone for full-band Monte Carlo simulation. They allow for simple and fast linear interpolation of the energy within the tetrahedrons and to calculate efficiently the particle group velocity and the density of states, three values needed very frequently during a full-band Monte Carlo simulation. Tetrahedral meshes offer a very good potential for refinement techniques. Simulation results in the high field regime show similar accuracy for properly refined meshes as for structured octree-based meshes with more than ten times the amount of tetrahedral elements. Simulations of electron mobility and mean electron energy in the low field regime show much better results for refined meshes than octree-based meshes, particularly for simulations with low lattice temperatures.

References

[1] D.N. Arnold, A. Mukherjee, L. Pouly, Locally adapted tetrahedral meshes using bisection, SIAM J. Sci. Comput. 22 (2) (2000) 431–448.
[2] B. Fischer, A full-band Monte Carlo charge transport model for nanoscale silicon devices including strain, Ph.D. Thesis, University Hannover, Germany (1999).

[3] P. Fleischmann, Mesh generation for technology CAD in three dimensions, Dissertation, Institut für Mikroelektronik, Technische Universität Wien, http://www.iue.tuwien.ac.at/phd/fleischmann (1999).
[4] T. Grasser, H. Kosina, S. Selberherr, VMC User Manual, http://www.iue.tuwien.ac.at/software/vmc, Austria (2003).
[5] C. Jacoboni, L. Reggiani, The Monte Carlo method for the solution of charge transport in semiconductors with application to covalent materials, Rev. Mod. Phys. 55 (3) (1983) 645–705.
[6] C. Jungemann, B. Meinerzhagen, Hierarchical Device Simulation, 1st ed., Springer, Wien New York, 2003.
[7] I. Kossaczký, A recursive approach to local mesh refinement in two or three dimensions, ELSEVIER, J. Comput. Appl. Math. (55) (1994) 275–288.
[8] G. Lehmann, M. Taut, On the numerical calculation of the density of states and related properties, Phys. Status Solidi B 54 (1972) 469–477.
[9] M. Lundstrom, Fundamentals of Carrier Transport, Cambridge University Press, United Kingdom, 2000.
[10] M. Rieger, P. Vogl, Electronic-band parameters in strained $Si_{1-x}Ge_x$ alloys on $Si_{1-y}Ge_y$ substrates, Phys. Rev. B 48 (19) (1993) 14276–14287.
[11] S. Smirnov, H. Kosina, M. Nedjalkov, S. Selberherr, A zero-field Monte Carlo algorithm accounting for the pauli exclusion principle, LSSC (2003) 185–193.